remote sensing

Article

A Comparison of Information Content at Microwave to Millimeter Wave Bands for Atmospheric Sounding

Xianjun Xiao [1,2] and Fuzhong Weng [1,2,*]

1 CMA Earth System Modeling and Prediction Centre (CEMC), Beijing 100080, China
2 State Key Laboratory of Severe Weather, Beijing 100081, China
* Correspondence: wengfz@cma.gov.cn

Abstract: The brightness temperatures and their Jacobians with respect to atmospheric temperature and humidity at the microwave to millimeter wave spectral bands from 23 GHz to 424 GHz are simulated with the ECMWF IFS-137 profiles as inputs to the Advanced Radiative transfer Modeling System (ARMS). The information content of temperature and humidity is then calculated individually through the Shannon entropy which is contributed by a-priori background information and observations. For a typical set of measurement uncertainties, a high information content for atmospheric temperature is mainly obtained from V band near 50–70 GHz, whereas that for water vapor comes from G band near 183 GHz and Y1 band near 380 GHz. The channels within the G band have a large temperature information content mainly for lower and middle layers of troposphere and the Y1 band has a relatively large humidity information content for the entire troposphere. A large measurement uncertainty can significantly reduce the information content of each band. Thus, to make a best use of the data from each band, it is important to reduce the instrument calibration noise and increase the accuracy in forward radiative transfer simulation.

Keywords: information content; microwave; millimeter wave; ARMS; entropy

check for updates

Citation: Xiao, X.; Weng, F. A Comparison of Information Content at Microwave to Millimeter Wave Bands for Atmospheric Sounding. *Remote Sens.* **2022**, *14*, 6124. https://doi.org/10.3390/rs14236124

Academic Editor: Steven C. Reising

Received: 5 September 2022
Accepted: 29 November 2022
Published: 2 December 2022

1. Introduction

Satellite-borne microwave atmospheric sounding instruments provide vital observations for environment monitoring and numerical weather model data assimilation. The principle of microwave sounding is largely based on the oxygen absorption lines for temperature profiling and the water vapor absorption lines for humidity profiling. Compared with infrared instruments, microwave instruments can "see" through clouds and precipitation and therefore are better suited to obtain all-sky atmospheric information, which is essential to the numerical weather prediction. Since the 1960s, a number of meteorological satellites have carried onboard microwave sounders for atmospheric sounding. The combination of the Microwave Sounding Unit (MSU) and the Infrared Atmospheric Sounder (HIRS), launched in 1978 in the United States, enabled remote sensing of the vertical temperature profile of the atmosphere with 4 channels at 50 GHz. Subsequently, the US launched SSM/I, SSM/T-1, SSM/T-2, and SSMIS in the DMSP program. SSM/T-1 was designed for atmospheric temperature, whereas SSM/T-2 is for atmospheric humidity. SSM/I and SSMIS, whose channels range from 19 GHz to 183 GHz, can get the information on cloud, rain, sea ice and snow cover, in addition to atmospheric profiles [1]. In NOAA satellite program, AMSU-A and AMSU-B are also carried onboard the operational environmental satellite NOAA-KLM series and replace MSU as the second generation of atmospheric sounding systems [2,3]. AMSU-A has 15 channels at 23–89 GHz. AMSU-B has five channels at 89–183 GHz. Europe has launched MetOp-A, MetOp-B and MetOp-C with the same microwave sounding system as that of U.S. environmental satellites. The latest generation of microwave sounding system onboard the Suomi National Polar-orbiting Partnership (SNPP) and NOAA-20 satellites is ATMS, which provides 22 more channels.

MetOp-SG is planned to be launched in 2023 with a high frequency channel at 229 GHz [3]. China's satellite microwave sounding system was developed more recently. The FY-3A polar-orbiting meteorological satellite, launched in 2008, carried microwave thermometer MWTS-1 and microwave hygrometer MWHS-1 for the first time to carry out atmospheric observations of cloudy and rainy areas. After two experimental satellites, FY-3A and FY-3B, the China Meteorological Administration (CMA) steadily upgraded the technology and later carried more advanced microwave sounding instruments on FY-3D and FY-3E satellites. The data collected were widely used in operational numerical weather prediction and research, demonstrating that microwave sounding data can greatly enhance numerical forecasting under both clear and cloudy conditions [4–13]. With the development of payload technology and considering the growing demand of microwave application, the CMA plans to launch the FY-4 geostationary Microwave Meteorological Satellite, carrying microwave instruments with more channels to perform observations at high temporal and spectrum resolution to further improve the numerical weather forecasting. The number of sounding channels on this satellite will be greatly increased compared to previous onboard microwave instruments. Hyperspectral sounding channels in the 50 GHz band and high-frequency 380 GHz and 424 GHz channels are also planned.

In the past, the observation system simulation experiment (OSSE) and assimilation experiments are widely utilized for exploring and evaluating the impacts of microwave instruments on forecasts. However, the contribution of the specific channels for existing and planned atmospheric sounders to the total information content is not fully understood. In recent years, the information content analysis is also developed for channel selection of satellite-borne infrared hyperspectral data for the data assimilation and is becoming a mature method for satellite applications [14,15]. By ranking the magnitude of channel information content, the channels with high information content (i.e., the subset of channels that contribute more to the observation system) can be preferentially selected according to specific applications. In assessing the microwave hyperspectral payloads, some scholars have also started to introduce the information content method into the channel selection [16–19]. This study first calculates the information content of all the channels in some important microwave spectral bands, so as to quantitatively evaluate the contribution of each channel, analyze the role of channels in the retrieval of atmospheric temperature and humidity profiles, and provide valuable references for the optimal configuration of channels on the application of future microwave observational data.

This paper is organized as follows: Section 2 introduces a fast radiative transfer model and dataset used in this paper. Section 3 provides a description of the scheme for calculating the channel information content. Section 4 analyzes the Jacobian function of the channels, which is the basis for the subsequent channel information content analysis. Section 5 is an analysis of the results of the channel information content. Finally, Section 6 provides a discussion and conclusion, and suggests the optimal configuration of channels for application.

2. Radiative Transfer Model and Profile Dataset

2.1. Radiative Transfer Model

The interaction between radiation energy and atmospheric media is characterized through gaseous absorption or particle scattering and the fast calculation for atmospheric radiative transfer is important in satellite remote sensing and data assimilation [20,21]. The model is used as an observational operator to establish the relationships between satellite microwave and infrared sounding radiances and atmospheric state variables, which can effectively assimilate satellite radiation data into the numerical prediction system (NWP). Internationally used rapid radiative transfer models are the Community Radiative Transfer Model (CRTM) [22], TIROS Operational Vertical Sounder (RTTOV) [23,24], and Advanced Radiative transfer Modeling System (ARMS) [25–27]. Most of these models consist of an atmospheric gas absorption module, an absorption scattering module for aerosols and clouds, a surface emission and reflection module, and a radiative transfer scheme, among which ARMS, as China's self-developed rapid radiative transfer model, contains some additional modules that consider the scattering of spherical and non-spherical aqueous particles and emission and scattering from rough ocean or land surfaces, and supports all instruments on board the Fengyun satellite [25]. The input parameters of the atmospheric gas absorption module include the atmospheric temperature, air pressure, and humidity profiles and five alternative atmospheric absorption calculation methods, which allow the calculation of the total gas absorption, the spectral absorption and the continuous absorption of water vapor. The parameters, such as wavelength, temperature, mean particle size, and mixing ratio of hydrometeor content, are used to calculate absorption and scattering cross section, and scattering phase functions. The surface emissivity module allows one to set the surface type as desired. The IFS-137 profile set selected for this study is more uniformly distributed globally, and the calculation is based on different surface types to calculate the land or ocean surface emissivity [26]. Parameters, such as temperature and humidity profiles, latitude and longitude, surface temperature, and 10-m wind speed extracted from IFS-137, were input, and the scanning angles were set to 0° or 60° according to the frequency of the channel (where the window channel is set to 60° and the other channels to 0°) to produce the temperature and humidity Jacobian for each channel.

2.2. NWP Profile Dataset

The atmospheric model profile data used for the calculation of Jacobian were extracted from the IFS-137 (The Integrated Forecast System, 137-levels) profile database of the European Centre for Medium-Range Weather Forecasts (ECMWF), which includes a representative set of 25,000 atmospheric profiles from global short-term forecasts in a 137-level vertical grid extending from the surface to 0.01 hpa. The database is divided into five subsets focusing on different sampling of temperature, specific humidity, ozone mixing ratio, cloud condensate, and precipitation [28,29]. The profile database is compiled from the short-range forecasts spanning the time period of 1 September 2013–31 August 2014. The forecasts are produced by the version Cy40r1 of the Integrated Forecasting System (IFS), which became operational at ECMWF on 19 November 2013 (earlier forecasts used in this work are from pre-operational testing period). In contrast to earlier releases of the ECMWF diverse profile database, the 137-level database puts an increased emphasis on preserving statistical properties of sampled distributions (i.e., including a realistic amount of frequently occurring atmospheric states). This is achieved by applying randomized selection to provide majority (90%) of profiles in the output database. The method applied in the production of the IFS-137 database benefits from two extensions to the earlier method. Firstly, a quality control step has been introduced to prevent unphysical profiles from entering the output database. Secondly, an option has been added to select a large number of profiles at random without the requirement on sufficient departure from all other selected profiles. A subset concentrating on temperature sampling was selected for this study (Figure 1).

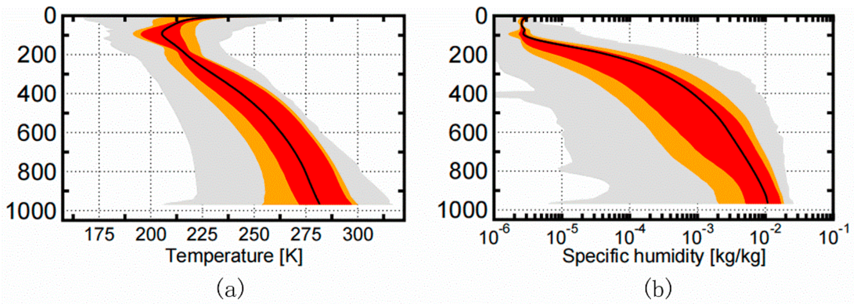

Figure 1. Distribution of (**a**) temperature and (**b**) specific humidity subsets in the IFS-137 profile set. Gray shading indicates the range constrained by minimum and maximum values, orange shading that constrained by 10th and 90th percentiles, and red shading that constrained by lower and upper quartiles (25th and 75th percentiles). Black solid line show the mean profile.

3. Channel Jacobian Analysis

The channels analyzed in this paper can be divided into three types according to the object of analysis: temperature sounding, humidity sounding, window channels that cooperate with cloud and rain analysis and window channels related to surface parameter retrieval. The Jacobian is the partial derivative of radiance with respect to the atmospheric parameters influencing that radiance. The Jacobian is fundamental in radiance assimilation as its magnitude and shape determine the magnitude and shape of the analysis increments. The sensitivity of channels at different frequencies to the atmospheric state variables is also determined by the shape of the Jacobians. The mean of the temperature and humidity Jacobians for all the profiles of IFS-137 profile set is represented in Figure 2.

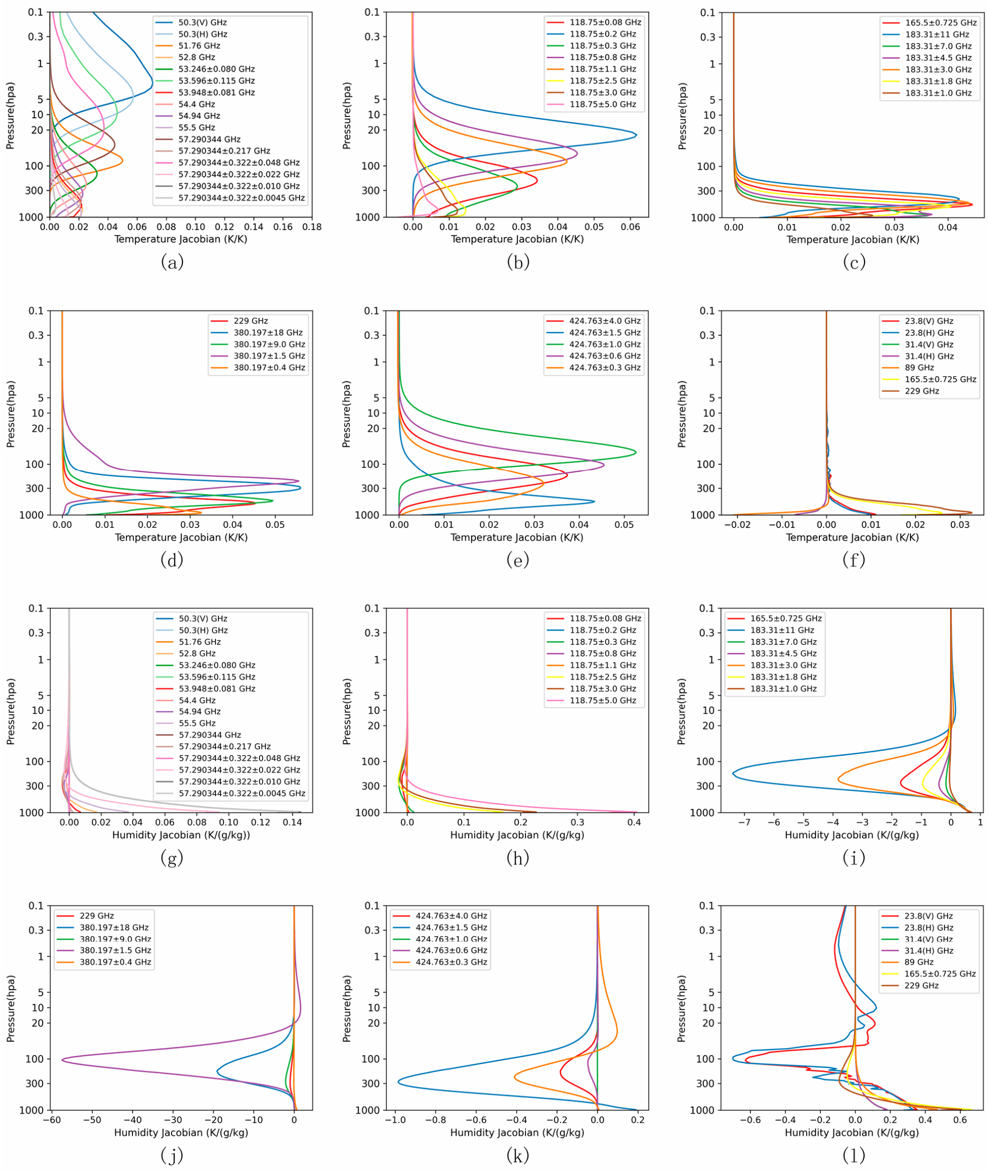

Figure 2. (**a**–**f**) Temperature and (**g**–**l**) humidity Jacobians at each spectral band.

In the microwave spectrum, only water vapor and molecular oxygen show significant absorption. Compared with the infrared spectrum, the microwave spectrum has only a limited number of absorption lines. Table 1 gives a description of the analyzed channel settings. In the Table 1, T denotes temperature and Q denotes humidity. The channels in the Table 1 are 46 channels, whose frequency is from 23 GHz to 424 GHz. There are 6 window channels that are 23.8 GHz, 31.4 GHz, 50.3 GHz, 89 GHz, 165 GHz, and 229 GHz which used to observe surface features and related cloud water or cloud ice parameters. The 60 GHz is the oxygen absorption band, which is almost transparent to water vapor, and 16 temperature sounding channels are set up near this spectrum. These channels are mainly temperature sensitive and not sensitive to water vapor. 8 channels were set up near 118 GHz and six channels near 183 GHz for sounding water vapor. 118 GHz and 183 GHz also have sensitivity to temperature. 118 GHz has a stronger Jacobian of temperature than 183 GHz in the lower troposphere. In the high frequency band with 380.197 GHz as the center of the water vapor absorption band are set up four channels to detect water vapor, and with 424.763 GHz as the center of the oxygen absorption band are set up five channels for temperature sounding. Due to the Riemann effect, the closer to the upper atmosphere, the denser the oxygen absorption lines are, implying a greater variation of transmittance with frequency. Therefore, the absorption varies even for the same channel at different heights.

Temperature and humidity are the basic quantities that characterize the thermal state of the atmosphere. The inhomogeneity of temperature distribution in the atmosphere forms cold and warm air masses that determine local atmospheric cooling and warming conditions, respectively. Water vapor in the atmosphere is necessary for the formation of clouds that cause rain, and it is very unevenly distributed in the atmosphere. To accurately forecast weather and climate conditions, accurate forecasts of temperature and water vapor conditions are indispensable, and later we calculate the temperature information content and humidity information content of each channel separately to quantify their contributions to temperature and water vapor, respectively.

Table 1. Characteristics of microwave and millimeter wave band and polarization.

Band	Number	Center Frequency (GHz)	Bandwidth (MHz)	Polarization	Sensitivity (K)	NEDT (K)	RTM Error (K)	Peak Height (hPa)	Sensitive Variable
K/Ka	1	23.8	270	V	0.5	0.25	2.0	1085.46	Window
	2	23.8	270	H	0.5	0.25	2.0	1085.46	Window
	3	31.4	180	V	0.5	0.3	2.0	1085.46	Window
	4	31.4	180	H	0.5	0.3	2.0	1085.46	window
V	5	50.3	180	V	0.5	0.4	0.1	1085.46	T
	6	50.3	180	H	0.5	0.4	0.1	1085.46	T
	7	51.76	400	H	0.5	0.3	0.1	1085.46	T
	8	52.8	400	H	0.5	0.25	0.1	972.329	T
	9	53.246 ± 0.080	2×140	H	0.5	0.4	0.1	814.871	T
	10	53.596 ± 0.115	2×170	H	0.5	0.25	0.1	672.43	T
	11	53.948 ± 0.081	2×142	H	0.5	0.4	0.1	525.476	T
	12	54.4	400	H	0.5	0.25	0.1	382.808	T
	13	54.94	400	H	0.5	0.25	0.1	266.444	T
	14	55.5	330	H	0.5	0.25	0.1	175.048	T
	15	57.290344 (f_0)	330	H	1	0.25	0.1	86.3757	T
	16	$f_0 \pm 0.217$	2×78	H	1	0.4	0.1	49.358	T
	17	$f_0 \pm 0.322 \pm 0.048$	4×36	H	1	0.6	0.1	30.6977	T
	18	$f0 \pm 0.322 \pm 0.022$	4×16	H	1.5	0.6	0.1	15.4439	T
	19	$f0 \pm 0.322 \pm 0.010$	4×8	H	1.5	0.8	0.1	6.4172	T
	20	$f0 \pm 0.322 \pm 0.0045$	4×3	H	2.5	1.2	0.1	3.0204	T
W	21	89	3000	V	0.5	0.2	2.0	1085.46	window

Table 1. *Cont.*

Band	Number	Center Frequency (GHz)	Bandwidth (MHz)	Polarization	Sensitivity (K)	NEDT (K)	RTM Error (K)	Peak Height (hPa)	Sensitive Variable
F	22	118.75 ± 0.08	2 × 20	H	2.5	2.0	1.5	30.6977	T
	23	118.75 ± 0.2	2 × 100	H	1.5	0.7	1.5	68.8325	T
	24	118.75 ± 0.3	2 × 165	H	1	0.7	1.5	92.8171	T
	25	118.75 ± 0.8	2 × 200	H	1	0.7	1.5	241.321	T
	26	118.75 ± 1.1	2 × 200	H	1	0.7	1.5	399.183	T
	27	118.75 ± 2.5	2 × 200	H	1	0.5	1.5	972.329	T
	28	118.75 ± 3.0	2 × 1000	H	1	0.5	1.5	1000.01	T
	29	118.75 ± 5.0	2 × 2000	H	1	0.5	1.5	1028.09	T
G	30	165.5 ± 0.725	2 × 1350	V	1	0.5	2.0	814.871	window
	31	183.31 ± 11	2 × 2000	H	0.5	0.4	1.5	790.081	Q
	32	183.31 ± 7.0	2 × 2000	H	0.5	0.4	1.5	741.757	Q
	33	183.31 ± 4.5	2 × 2000	H	0.5	0.5	1.5	672.43	Q
	34	183.31 ± 3.0	2 × 1000	H	1	0.5	1.5	525.476	Q
	35	183.31 ± 1.8	2 × 1000	H	1	0.6	1.5	450.797	Q
	36	183.31 ± 1.0	2 × 500	H	1	0.7	1.5	399.183	Q
J	37	229	2000	V	1	0.7	2.0	814.8 + C86:C9571	Window
Y1	38	380.197 ± 18.0	2 × 2000	H	1	1.2	1.5	565.346	T/Q
	39	380.197 ± 9.0	2 × 2000	H	1	1.2	1.5	487.295	T/Q
	40	380.197 ± 1.5	2 × 500	H	2	1.2	1.5	307.068	T/Q
	41	380.197 ± 0.4	2 × 200	H	2.5	1.2	1.5	266.444	T/Q
Y2	42	424.763 ± 4.0	2 × 1000	H	1	1.2	1.5	545.199	T
	43	424.763 ± 1.5	2 × 600	H	1.5	1.2	1.5	450.797	T
	44	424.763 ± 1.0	2 × 400	H	2	1.2	1.5	185.169	T
	45	424.763 ± 0.6	2 × 200	H	2.5	1.2	1.5	106.627	T
	46	424.763 ± 0.3	2 × 100	H	3	1.2	1.5	63.5574	T

4. Information Content Calculation

In information theory, the system is in a state of complete disorder, we know the least about the system, and entropy is at its maximum. The reduction in the information entropy of the system due to the addition of observations is defined as the information content of the observations. The amount of information brought to the system by the observation is mainly manifested by a decrease in the estimation error of the system and an increase in the certainty of the system. The ability of the observations to optimize the system is related to the quality of the observations themselves, as well as the model performance. The quality of the observation itself and the characteristics of its influence on the system can be expressed by the observation error covariance matrix R. The model performance is the prior information of the system, expressed as the background error covariance matrix of the system, which is denoted by B in the text. In this sense, the reduction of information entropy due to observation is the improvement of signal-to-noise ratio due to observation. Therefore, the information content ER of the observation is the difference between the information entropy S of the prior probability $P(x)$ and the posterior probability $P(x|y)$. In reference to the paper of Rabier [15], we present the following equation,

$$ER = S(P(x)) - S(P(x\big|y)) = -\frac{1}{2}ln(\frac{|\boldsymbol{A}|}{|\boldsymbol{B}|}), \tag{1}$$

where x is the atmospheric state vector to be inverted, y is the observed vector, and A is the analytical error covariance matrix. The analytical error of the system changes during the change of the observations added to the system. The analytical error $\boldsymbol{A}$ is calculated as follows:

$$\mathbf{A}=(\mathbf{B}^{-1}+\mathbf{H}^{\mathbf{T}}\mathbf{R}^{-1}\mathbf{H})^{-1}, \tag{2}$$

where H are the Jacobians of temperature and humidity, which are from the fast radiative transfer model ARMS. The background error covariance B is derived from the 137-layer error profile of the ECMWF model global sample temperature and humidity. Jacobians of profiles output from ARMS have fixed levels, i.e., 95 levels. When calculating information content using Jacobians, we interpolated the B matrix to the same number of levels as Jacobians. The background error variance after processing is shown in Figure 3. The observation error variance R was obtained according to the NEdT and the estimated error of radiative transfer model [30,31]. The NEdT of most of the channels at K/Ka band, V band and G band are set according to AMSU/MHS. For the rest of the channels at these bands, we set the NEdT reference to ATMS. The NEdT of the channels at F band are coming from FY-3C MWHS-2. There are two channels whose NEdT are from Metop-SG MWS. For those high frequency channels at Y1 band and Y2 band, we just give a rough estimate. For computational convenience, the observation error covariance matrix here is a diagonal matrix (i.e., the correlation between channels was not considered).

The channel information content was calculated using an iterative approach. Based on the initial background error and observation error, the information content of each channel in the channel subset was first calculated, the information content was ranked, and the channel with the largest increase was the first selected channel to be retained in the system. The analysis error was then calculated, and the background error was updated with this analysis error. That is to say, B is substituted with the calculated A in the next step to select the second channel. In the second step, each of the remaining channels was added to the system individually, and the information content was calculated once at a time. The calculated information content was sorted so that the channel with the largest increase in the information content of the system was selected and retained in the system. B is substituted with the new A again. The second step was repeated, and the information content of the remaining channels was calculated until all channels were covered. Finally, according to the order in which the channels were added to the system, the information content of the channels was also sorted from highest to lowest. In order to make the calculation of channel information content statistically significant, the channel information content calculated in this paper was the profile-averaged channel information content. The profile set is composed of the 5000 datasets of NWPSAF introduced above. In the actual calculation of channel information content, we found that the trend of channel information content and channel ranking were the same for 5000 profiles and 200 profiles. Therefore, in the end, we only used 200 profiles in the actual calculation for simplicity. These 200 profiles were selected evenly among the 5000 profiles.

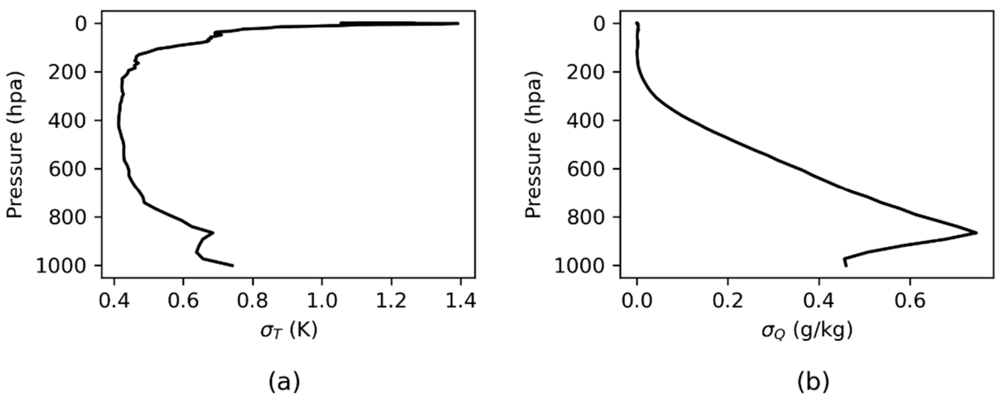

Figure 3. Background error standard deviation for (**a**) temperature (σ_T) and (**b**) humidity (σ_Q).

5. Information Content Analysis

According to the calculation scheme in Section 4, the total channel information content gradually increases as the number of channels increase. Figure 4 shows the information content of temperature and humidity against channel. The information content of temperature increases relatively slowly with the number of channels, while the information content of humidity goes up rapidly within the first 10 channels, and then becomes saturated. The temperature analysis error is reduced throughout the atmosphere with respect to the background error covariance, and the standard deviation of the temperature error is reduced by approximately 1.5% on average. The largest reduction is in the layer near 600 hPa by 2.4%. The reduction of the humidity analysis error relative to the background error is located near 850 hPa and 500 hPa, with an average reduction of 17% and 12%, respectively (Figure 5).

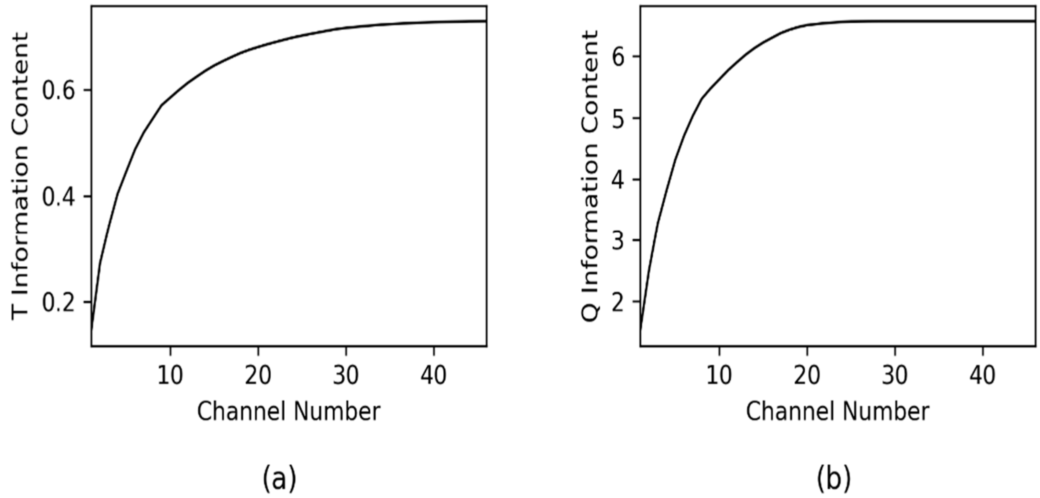

Figure 4. Information content of (**a**) temperature and (**b**) humidity variation with the increase of channel number.

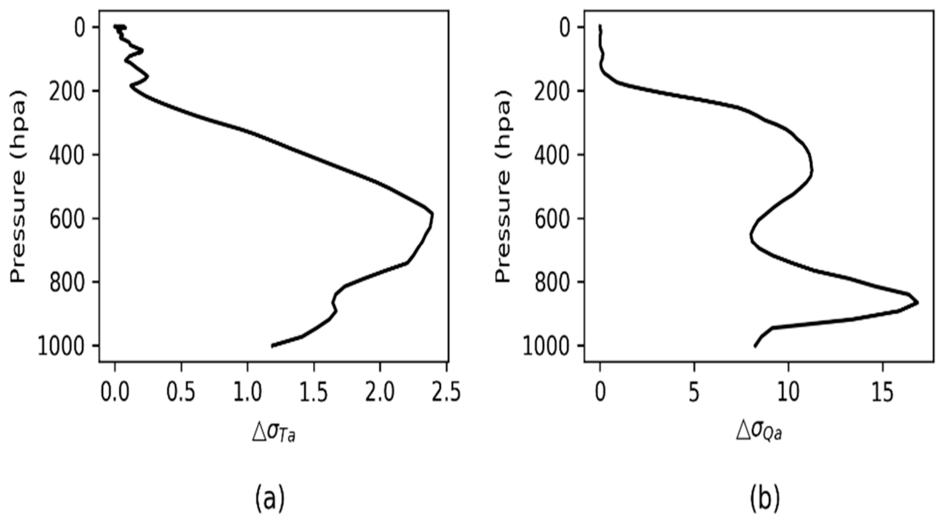

Figure 5. Analysis error standard deviation reduction in percentage with respect to the background error for (**a**) temperature ($\Delta\sigma_T$) and (**b**) humidity ($\Delta\sigma_Q$) at all 8 spectrum bands.

The nature of the sounding channel of a remote sensing instrument can be visualized by its Jacobian function. It is generally the case that the larger the value of the Jacobian function, the larger the contribution of the channel. The most commonly used temperature sounding band is 60 GHz (V band), and the 118 GHz (F band), 183 GHz (G band), 229 GHz (J band), 380 GHz (Y1 band), and 424 GHz (Y2 band) bands from its temperature Jacobian function are found to be sensitive to temperature as well. The temperature and humidity information content of each band is calculated (Figure 6). It is found that the V band has the much more higher temperature information content, and the G band has a slightly higher value. The rest of the bands almost have no contribution to the temperature. The high value channels of humidity information content are mainly at G band, V band, and Y1 band. In addition, the humidity information content of window channel 23.8 GHz, which contributes significantly to the atmospheric bottom layer humidity, is bigger than those of the rest of the bands.

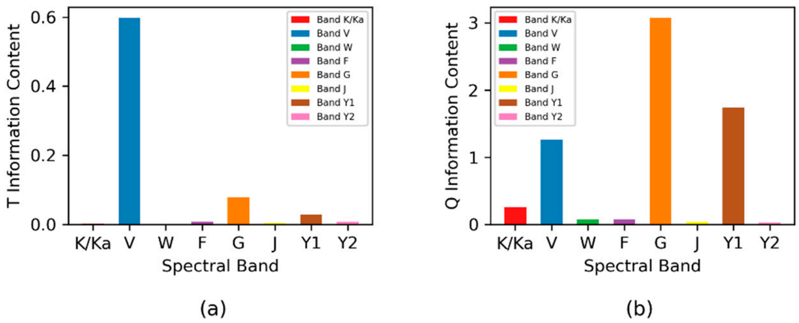

Figure 6. Information content of (**a**) temperature and (**b**) humidity at each spectrum band.

5.1. Information Content Contribution of 118 GHz

The band at 118 GHz (F band) is unique for MWHS-2 in FY-3C, FY-3D and FY-3E satellites. So far, there is still a lack of in-depth study on the benefit to the atmospheric sounding from F band. Using the information content, we can validate the relative contributions of these channels, given our best knowledge of F band technology. Here, we define a channel subset name as a group. Group 1 includes K/Ka band, V band, W band and G band the same as those channels available from the other microwave payloads. The second channels subset is named as group 2 which is group 1 plus F band. The temperature information content is calculated to check the performance of the 118 GHz under clear sky. Figure 7 shows the temperature information content increase about by 1% after adding F band. The temperature analysis increments between 500 hPa and 850 hPa are improved more obviously (Figure 7c). The humidity information content increment is also approximately 1%, mainly near at 850 hPa (Figure 8). So, the contribution of F band is limited. We expect that the improvement may be more significant according to the combination effect of temperature and humidity, which is not accounted for in this paper.

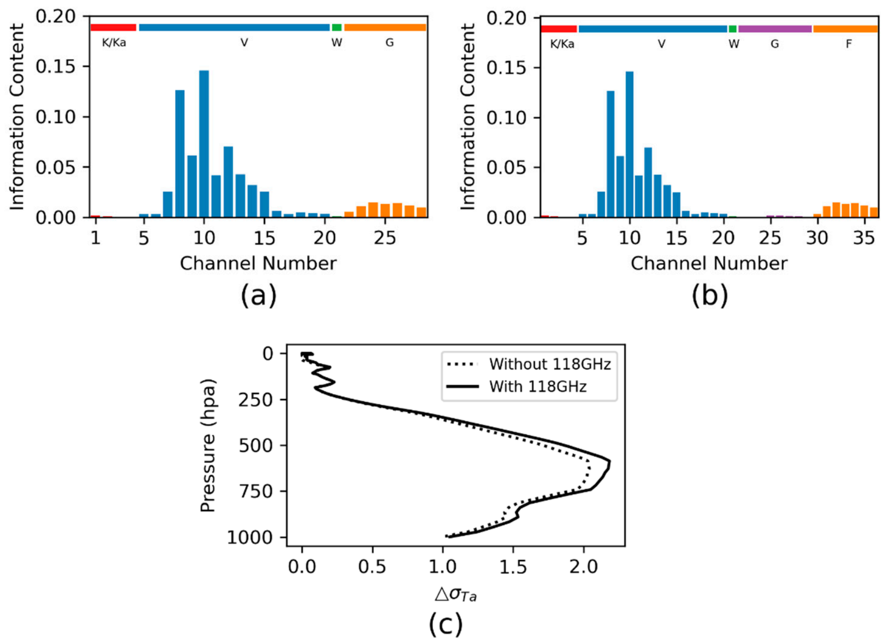

Figure 7. (**a**) Temperature information content of group 1. (**b**) Group 1 + F Band. (**c**) The temperature analysis increment ($\Delta\sigma_T$) in percentage.

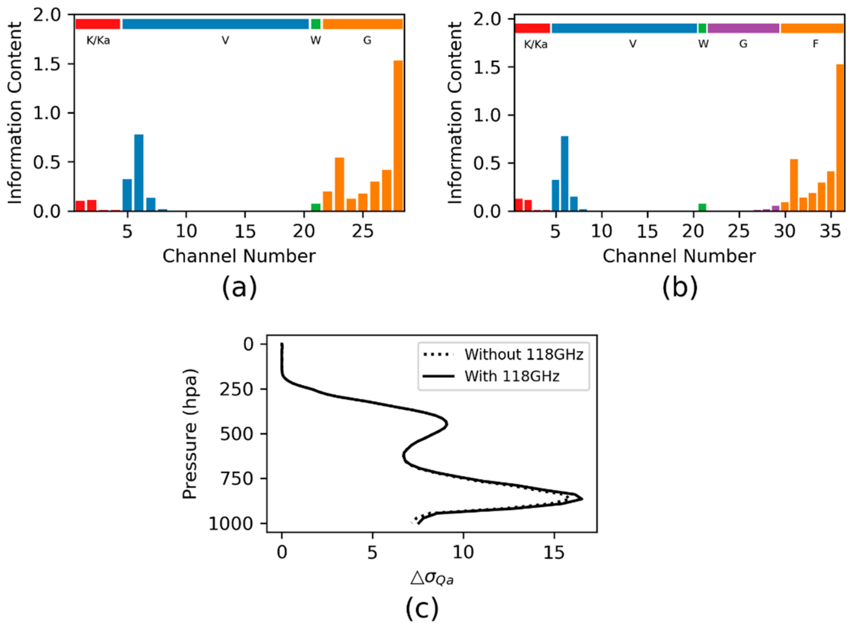

Figure 8. (**a**) Humidity information content of group 1. (**b**) Group 1 + F band, and (**c**) The humidity analysis increment ($\Delta\sigma_Q$) in percentage.

5.2. Information Content Analysis for Millimeter Wave Bands

J band, Y1 band, and Y2 band are in satellite mission plan of many countries because good performance enhancement is expected from these bands. It is important to understand their additional benefits for atmospheric sounding. The temperature information content at these bands is not significant as analyzed before, which is represented in Figure 9a,c. Figure 9b,d depicts the contribution of each band to humidity. We can see that band Y2 shows improved humidity in the bottom troposphere, while Y1 band shows improved humidity above 500 hPa. The humidity error standard deviation is decreased by 8% at most with band Y1, while more than 3% with band Y2. The contribution of band J is much small compared with the other two bands and can be ignored.

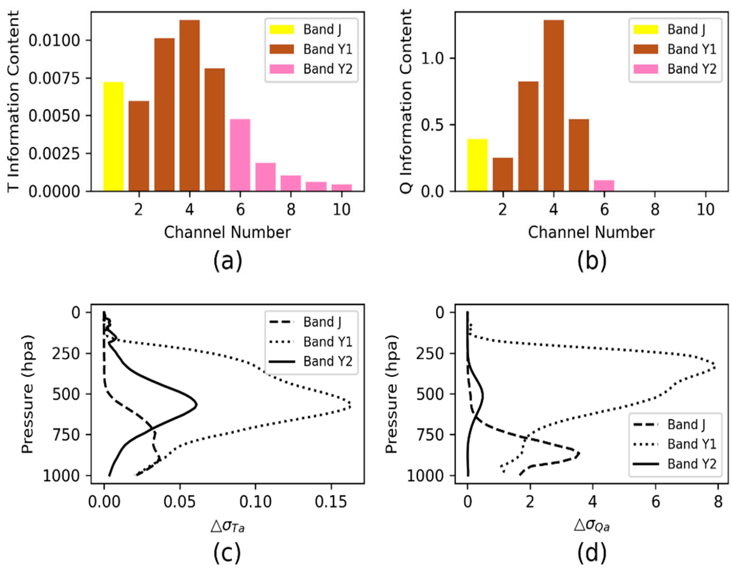

Figure 9. Temperature information content and the analysis increments at millimeter wave bands. (**a**,**b**) the temperature and humidity information content respectively. (**c**,**d**) temperature ($\Delta\sigma_T$) and humidity analysis increments ($\Delta\sigma_Q$) in percentage at each band respectively.

5.3. Impacts of the Observation Errors on the Information Content

As shown in Equation (1), channel information content is determined by the channel Jacobian, background error and observation error. Two sources of observational errors include instrument noise (NEdT) and radiative transfer simulations. In the last two columns of Table 1 give the NEdT and radiative transfer simulation errors of each channel, which comes from the consensus of previous studies. The errors of V band are increased with respect to the error NEDT + RTM by 0.5 K, 1.0 K and 1.5 K when we analyze the variation of the temperature information content at this band. The errors of F band and G band are decreased with respect to the error NEDT + RTM by 0.5 K, 1.0 K, and 1.5 K when we analyze the variation of the temperature information content at the two bands. Figure 10 depicts the influence of temperature information content on the variation of observation error. The temperature information content at V band is very sensitive to the variation of observation errors. The radiance error increases by 0.5 K, and the analysis increment of temperature rapidly decreases from more than 1.5% to 0.4%. The original temperature information content of F band is small, and not sensitive to the reduction of error. The error of G band is reduced by 1 K, the temperature analysis increment increases to 1.7%, and the contribution to temperature becomes significant.

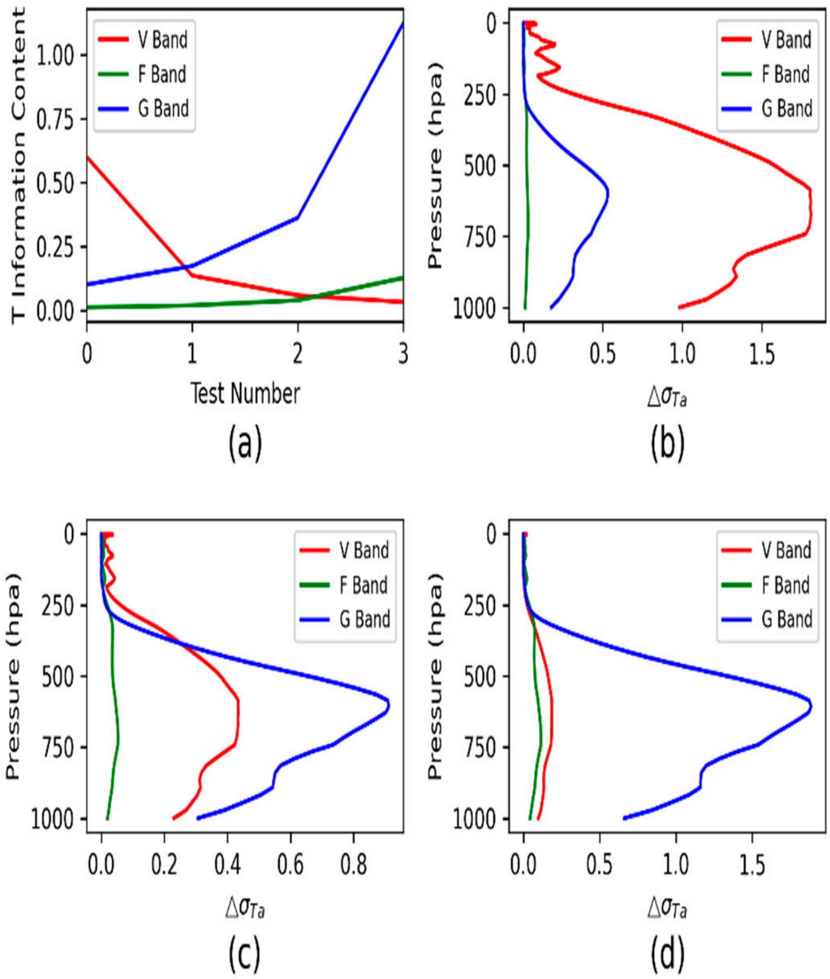

Figure 10. (**a**) Temperature information content with respect to test 0, 1, 2, 3, which represent the error increase of V band (red line) or decrease of F band and G band (green line and blue line) by 0, 0.5 K, 1.0 K, 1.5 K respectively. (**b**–**d**) The temperature analysis increment ($\Delta\sigma_{T_a}$) in percentage when the error increase (red line) or decrease (green line and blue line) by 0 K, 0.5 K and 1.0 K respectively.

The humidity information content of V band changes rapidly with the increase of error. The error increases by 0.5 K, and the humidity information content decreases by more than 5% (Figure 11). When the error of F band increases by 0.5 K, the humidity information increment only decreases by 1%, and the humidity information increment of G band decreases by about 0.5%. The humidity information increment decreases by more than 1% for every 0.5 K increase in the error at F band and G band. The decrease at F band is slightly faster. The humidity information content increase by 3% for every 0.5 K decrease in the error at F band and G band (Figure 12).

The information content of the V band is sensitive to observation errors, so it is important to maintain the high quality of the instrument. In this frequency band, if the observation error increases by 0.5 K, it will not provide effective temperature information content to the NWP, only humidity information. If the error of G band can be reduced by 1.5 K, it will perform as good as the V band in temperature sounding. Because of the low accuracy of the numerical model for atmospheric humidity simulation, even if the observation error at F band and G band increases by more than 1.5 k, it still contributes significantly to humidity.

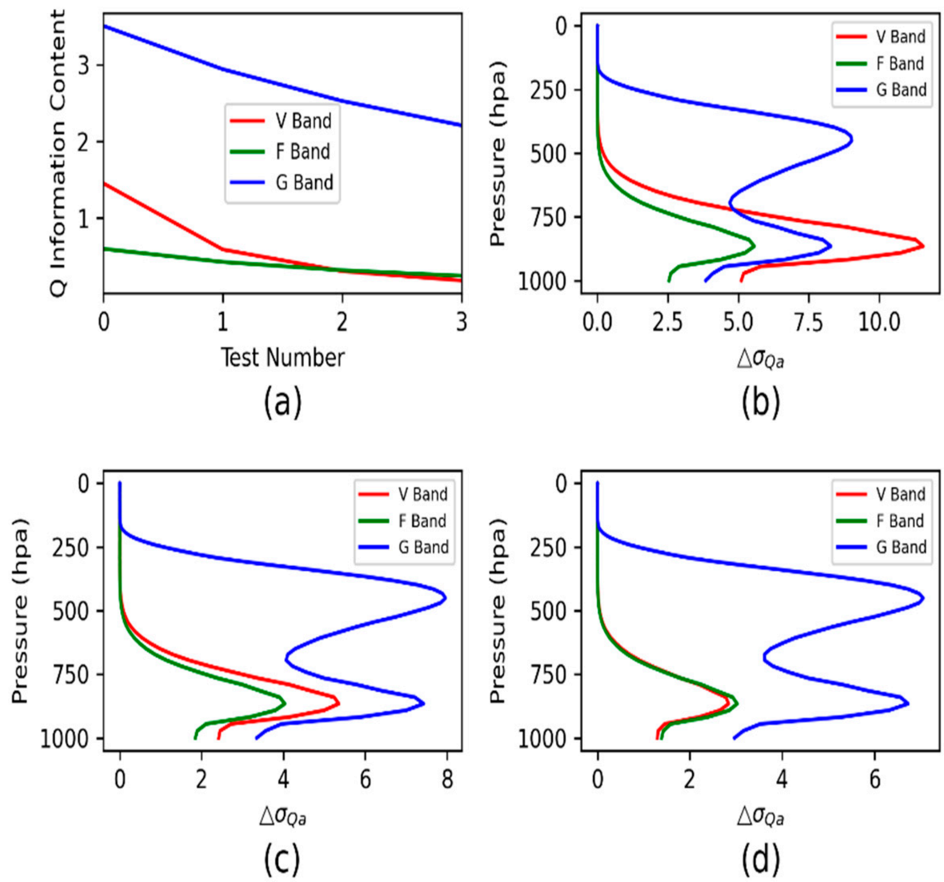

Figure 11. (**a**) The humidity information content with respect to test 0, 1, 2, 3, which represent the error increase of V band, F band and G band by 0, 0.5 K, 1.0 K, 1.5 K respectively. (**b**–**d**) The humidity analysis increment ($\Delta\sigma_{Q_a}$) in percentage when the error increase by 0.0 K, 0.5 K and 1.0 K respectively.

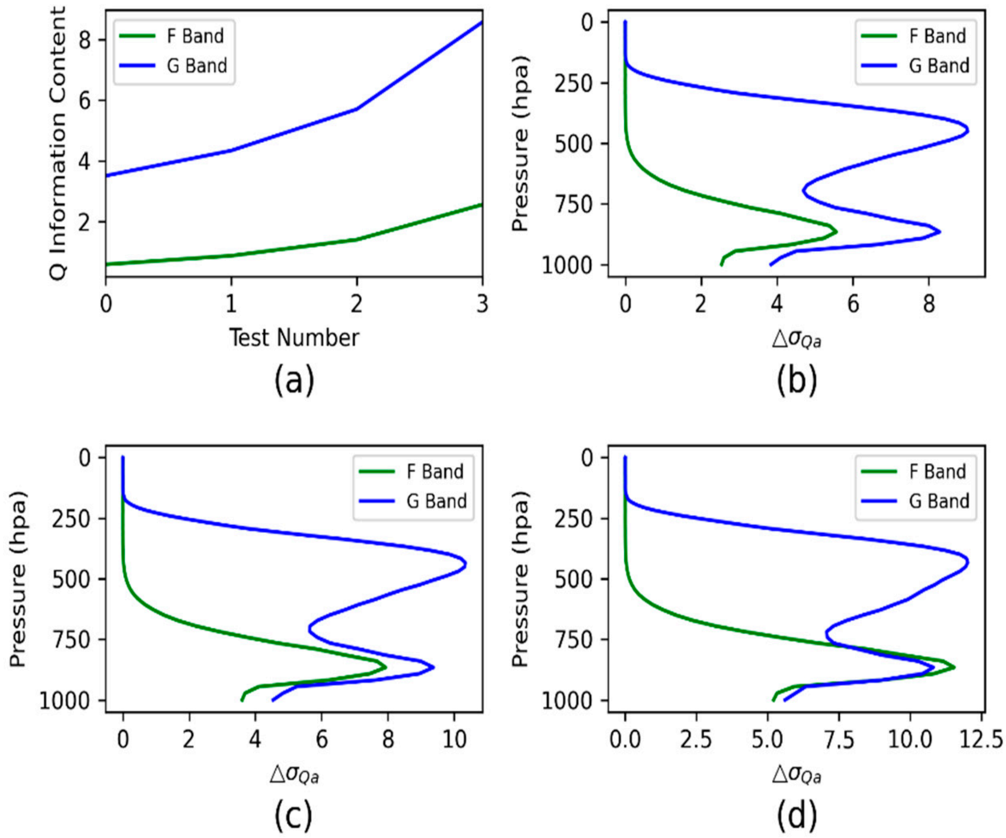

Figure 12. (**a**) The humidity information content with respect to test 0, 1, 2, 3, which represent the error decrease of F band and G band by 0, 0.5 K, 1 K, 1.5 K respectively. (**b–d**) The humidity analysis increment ($\Delta\sigma_{Q_a}$) in percentage when the error decrease by 0 K, 0.5 K and 1.0 K respectively.

6. Summary and Conclusions

In this paper, an information content of microwave to millimeter bands for atmospheric sounding is assessed. The analysis focuses on the temperature and humidity information content under clear sky conditions. The results of the analysis show that there is a significant difference in the effect of the contribution of each band to the temperature and humidity. This difference is mainly determined by a combination of the channel Jacobians and the background errors of temperature and humidity. The channels with the greatest temperature information content are mainly at V band, and those with the greatest humidity information are located within V band, G band, and Y1 bands. The different peak heights of the weighting functions of the channels lead to significant differences in the contributions of the channels at different layers of the atmosphere. The contribution of F band is not significant compared with the available channels in the current other payloads under the clear sky conditions according to the information content analysis. The millimeter wave channels at band J, band Y1, and band Y2 which have a higher spatial resolution, is suitable for small satellites. The information content analysis at these bands shows their values to humidity sounding. As a result, we suggest that the use of several high information content bands at the V band, G band, and Y1 band should be focused on the assimilation of clear sky radiation data in NWP applications. According to the analysis of impact of observational error on the information content, we found that G band has a relatively large humidity information content compared with those channels at other bands even with the large observation errors.

The channel information content provides a quantitative estimate of the total contribution of each channel, while the analytical increments obtained in the channel information content calculation provide a further quantitative estimate of the vertical distribution of the channel contribution. In the instrument design phase prior to satellite launch, having the channel information content from NEdT of the instrument can effectively help in assessing the benefits of the payload and can provide a useful reference for subsequent instrument design and future applications. However, for a cloudy atmosphere, the analysis of the channel information content is very complex, and the conclusions could be significantly different from this work. Our further work will analyze the information content of microwave channels under cloudy and rainy conditions to fully evaluate the performance of microwave instruments.

Author Contributions: Conceptualization, F.W.; methodology, X.X.; writing—original draft preparation, F.W.; review and editing, F.W. All authors have read and agreed to the published version of the manuscript.

Funding: This research was funded by the National Key Research and Development Program of China (2021YFB3900400) and the National Natural Science Foundation of China (U2142212).

Data Availability Statement: Atmospheric profiles are available from ECMWF.

Acknowledgments: We thank the reviewers and editors for their insightful comments.

Conflicts of Interest: The authors declare no conflict of interest.

References

1. Yan, B.H.; Weng, F.Z. Intercalibration between special sensor microwave imager/sounder and special sensor microwave imager. *IEEE Trans. Geosci. Remote Sens.* **2008**, *46*, 984–995.
2. Parkinson, C.L. Aqua: An Earth-observing satellite mission to examine water and other climate variables. *IEEE Trans. Geosci. Remote Sens.* **2003**, *41*, 173–183. [CrossRef]
3. Saunders, R.W.; English, S.J.; Jones, D.C. AMSU-B: A new tool for atmospheric research. In *Proceedings Volume 2313, Microwave Instrumentation and Satellite Photogrammetry for Remote Sensing of the Earth*; SPIE: Bellingham, WA, USA, 1994. [CrossRef]
4. Carminati, F.; Atkinson, N.; Candy, B.; Lu, Q.F. Insights into the microwave instruments onboard the Fengyun 3D satellite: Data quality and assimilation in the Met Office NWP system. *Adv. Atmos. Sci.* **2021**, *38*, 1379–1396. [CrossRef]
5. Bormann, N.; Duncan, D.; English, S.; Healy, S.; Lonitz, K.; Chen, K.; Lawrence, H.; Lu, Q. Growing operational use of FY-3 data in the ECMWF system. *Adv. Atmos. Sci.* **2021**, *38*, 1285. [CrossRef]
6. Zhang, P.; Yang, J.; Wang, J.; Yu, X. Preface to the special issue on Fengyun Meteorological Satellites: Data, application and assessment. *Adv. Atmos. Sci.* **2021**, *38*, 1265. [CrossRef]
7. Carminati, F.; Migliorini, S. All-sky data assimilation of MWTS-2 and MWHS-2 in the Met Office Global NWP System. *Adv. Atmos. Sci.* **2021**, *38*, 1682. [CrossRef]
8. Zhang, P.; Lu, Q.; Hu, X.; Gu, S.; Yang, L.; Min, M.; Chen, L.; Xu, N.; Sun, L.; Bai, W.; et al. Latest progress of the Chinese Meteorological Satellite Program and core data processing technologies. *Adv. Atmos. Sci.* **2019**, *36*, 1027–1045. [CrossRef]
9. Li, J.; Liu, G.Q. Direct assimilation of Chinese FY-3C microwave temperature sounder-2 radiances in the global GRAPES system. *Atmos. Meas. Tech.* **2016**, *9*, 3095–3113. [CrossRef]
10. Lu, Q.F.; Lawrence, H.; Bormann, N.; English, S.; Lean, K.; Atkinson, N.; Bell, W.; Carminati, F. An Evaluation of FY-3C Satellite Data Quality at ECMWF and the Met Office, European Centre for Medium-Range Weather Forecasts. 2015. Available online: https://www.ecmwf.int/sites/default/files/elibrary/2015/14692-evaluation-fy-3c-satellite-data-quality-ecmwf-and-met-office.pdf (accessed on 1 September 2022).
11. Lindskog, M.; Dybbroe, A.; Randriamampianina, R. Use of microwave radiances from Metop-C and Fengyun-3 C/D satellites for a northern European limited-area data assimilation system. *Adv. Atmos. Sci.* **2021**, *38*, 1415. [CrossRef]
12. Xiao, H.Y.; Han, W.; Wang, H.; Wang, J.; Liu, G.; Xu, C. Impact of FY-3D MWRI radiance assimilation in GRAPES 4DVar on forecasts of Typhoon Shanshan. *J. Meteor. Res.* **2020**, *34*, 836–850. [CrossRef]
13. Maddy, E.S.; Bunin, S.; Mikles, V.J.; Shahroudi, N.; Shiotani, B.; Boukabara, S.-A. Temperature and Moisture Sounding Performance of Current and Prospective Microwave Instruments under All-Sky Conditions. *Remote Sens.* **2022**, *14*, 1624. [CrossRef]
14. Collard, A.D. Selection of IASI channels for use in numerical weather prediction. *Q. J. R. Meteorol. Soc.* **2007**, *133*, 1977–1991. [CrossRef]
15. Rabier, F.; Fourrié, N.; Chafäi, D.; Prunet, P. Channel selection methods for Infrared Atmospheric Sounding Interferometer radiances. *Q. J. R. Meteorol. Soc.* **2002**, *128*, 1011–1027. [CrossRef]
16. Mahfouf, J.-F.; Birman, C.; Aires, F.; Prigent, C.; Orlandi, E.; Milz, M. Information content on temperature and water vapour from a hyper-spectral microwave sensor. *Q. J. R. Meteorol. Soc.* **2015**, *141*, 3268–3284. [CrossRef]
17. Michele, S.D.; Bauer, P. Passive microwave radiometer channel selection based on cloud and precipitation information content. *Q. J. R. Meteorol. Soc.* **2006**, *132*, 1299–1323. [CrossRef]
18. Sahoo, X.; Bosch-Lluis, S.; Reising, S.C.; Vivekanandan, J. Radiometric Information Content for Water Vapor and Temperature Profiling in Clear Skies Between 10 and 200 GHz. *IEEE J. Sel. Top. Appl. Earth Obs. Remote Sens.* **2015**, *8*, 859–871. [CrossRef]

19. Jde Torrella, M.G.; Camps, A. On the Amount of Information Content in Microwave Radiometry for Wet Delay Estimation. *IEEE J. Sel. Top. Appl. Earth Obs. Remote Sens.* **2017**, *10*, 3107–3113. [CrossRef]
20. Weng, F.; Liu, Q. Satellite data assimilation in numerical weather prediction models. part I: Forward radiative transfer and Jacobian modeling in cloudy atmospheres. *J. Atmos. Sci.* **2003**, *60*, 2633–2646. [CrossRef]
21. Weng, F.Z. Advances in radiative transfer modeling in support of satellite data assimilation. *J. Atmos. Sci.* **2007**, *64*, 3799–3807. [CrossRef]
22. Spurr, R.J.D.; Kurosu, T.P.; Chance, K.V. A linearized discrete ordinate radiative transfer model for atmospheric remote-sensing retrieval. *J. Quant. Spectrosc. Radiat. Transf.* **2001**, *68*, 689–735. [CrossRef]
23. Saunders, R.; Matricardi, M.; Brunel, P. An improved fast radiative transfer model for assimilation of satellite radiance observations. *Q. J. R. Meteorol. Soc.* **1999**, *125*, 1407–1425. [CrossRef]
24. Saunders, R.; Hocking, J.; Turner, E.; Rayer, P.; Rundle, D.; Brunel, P.; Vidot, J.; Roquet, P.; Matricardi, M.; Geer, A.; et al. An update on the RTTOV fast radiative transfer model (currently at version 12). *Geosci. Model Dev.* **2018**, *11*, 2717–2737. [CrossRef]
25. Weng, F.; Yu, X.; Duan, Y.; Yang, J.; Wang, J. Advanced Radiative transfer Modeling System (ARMS): A new-generation satellite observation operator developed for numerical weather prediction and remote sensing applications. *Adv. Atmos. Sci.* **2020**, *37*, 131–136. [CrossRef]
26. Yang, J.; Ding, S.; Dong, P.; Bi, L.; Yi, B. Advanced Radiative transfer Modeling System developed for satellitedata assimilation and remote sensing applications. *J. Quant. Spectrosc. Radiat. Transf.* **2020**, *251*, 107043. [CrossRef]
27. Shi, Y.N.; Yang, J.; Weng, F. Discrete Ordinate Adding Method (DOAM), a new solver for Advanced Radiative transfer Modeling System (ARMS). *Opt. Express* **2021**, *29*, 4700–4720. [CrossRef] [PubMed]
28. Eresmaa, R.; Mcnally, A.P. Diverse profile datasets from the ECMWF 137-level short-range forecasts. *NWP SAF NWPSAF-ECTR-017* **2014**, *10*, 4476–8963.
29. Chevallier, F.; Di Michele, S.; Mcnally, A.P. *Diverse Profile Datasets from the ECMWF 91-Level Short-Range Forecasts*; European Centre for Medium-Range Weather Forecasts: Reading, UK, 2006.
30. Weng, F.; Zou, X.; Wang, X.; Yang, S.; Goldberg, M.D. Introduction to Suomi national polar-orbiting partnership advanced technology microwave sounder for numerical weather prediction and tropical cyclone applications. *J. Geophys. Res.* **2012**, *117*, D19112. [CrossRef]
31. Moradi, I.; Goldberg, M.; Brath, M.; Ferraro, R.; Buehler, S.A.; Saunders, R.; Sun, N. Performance of radiative transfer models in the microwave region. *J. Geophys. Res. Atmos.* **2020**, *125*, e2019JD031831. [CrossRef]